# Measuring Fingertip Forces by Imaging the Fingernail

Yu Sun, John M. Hollerbach*
School of Computing
University of Utah

Stephen A. Mascaro†
Department of Mechanical
Engineering
University of Utah

## Abstract

This paper presents an external camera method for measuring fingertip forces by imaging the fingernail and surrounding skin. This method is an alternative to the photoplethysmograph sensor originally developed by one of the authors. A 3D model of the fingernail surface and skin is obtained with a stereo camera and laser striping system. Subsequent images from a single camera are registered to the 3D model by adding fiducial markings to the fingernail. Calibration results with a force sensor show that the measurement range depends on the region of the fingernail and skin. A Bayesian method is developed to predict fingertip force given coloration changes. Preliminary accuracy results for normal and shear force measurement are presented. In comparison to the results using the photoplethysmograph fingernail sensor, our results are more accurate and double the range of forces that can be transduced, all the way up to the saturation level.

**CR Categories:** H.5.2 [INFORMATION INTERFACES AND PRESENTATION]: User Interfaces—Haptic I/O;

**Keywords:** fingertip force, fingernail, coloration, image registration, Bayesian

## 1 Introduction

The use of coloration change in the fingernail to predict fingertip force was originally proposed by Mascaro and Asada [6]. The blood flowing under the fingernail is affected by the pressure at the fingerpad, and the coloration change in the fingernail provides a surprisingly good transduction of fingerpad force [7]. Shear forces as well as normal forces can be measured, although there is coupling between them [8].

To image the fingernail, Mascaro and Asada [6] devised a *photoplethysmograph sensor* comprised of an array of 6 LEDs to illuminate the fingernail and an array of 8 photodetectors to measure the coloration. These arrays are embedded in an epoxy substrate shaped like an artificial fingernail (Figure 1), which is individually fitted and attached to a subject's fingernail. Wires are routed out for interface with a computer. Sensor response was linear up to 1 N normal force and beyond 1 N there was a nonlinear leveling off [8]. With a linear model, the sensor predicted normal force to within 1 N accuracy in the range of 2 N and shear force to within 0.5 N accuracy in the range of 3 N.

In current grasping studies, instrumented objects are typically created that incorporate miniature 6-axis force/torque sensors at predefined grasp points [12]. The subject is not free to grasp an object in different ways or to change grasp

---

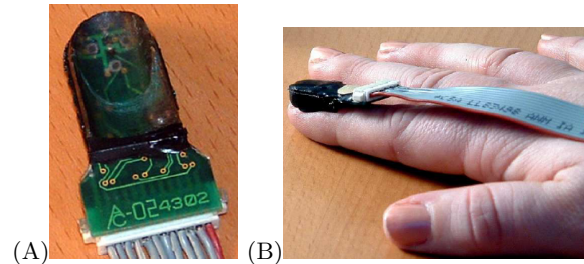*e-mail: {ysun,jmh}@cs.utah.edu

†e-mail:smascaro@mech.utah.edu

Figure 1: (A) The underside of the photoplethysmograph fingernail sensor. (B) The sensor attached to the fingernail.
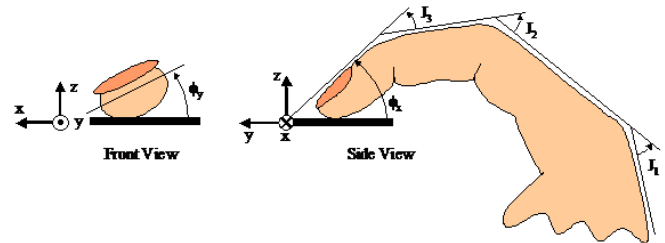


Figure 2: Contact conditions that influence coloration include normal force $f_z$, shear forces $f_x$ and $f_y$, fingertip orientation $\phi_x$ (pitch) and $\phi_y$ (roll), and finger joint angle $J_3$.

points. The fingernail-based force sensing technique has the great advantage that objects do not have to be instrumented and everyday objects can be used. There is no constraint on how a subject changes grasp points.

The need to fabricate sensors fitted to each fingernail is currently a disadvantage. Other limitations are the sparse sampling of the fingernail and the lack of imaging of the surrounding skin, whose coloration change we have found to transduce fingertip force well also. Besides normal and shear forces, other factors that influence fingernail coloration include the contact orientation, the curvature of the contact, and the DIP joint angle (Figure 2). They all combine to affect the coloration pattern, but it is asking a lot of a fixed sparse sampling of the fingernail image to separate the influences of these factors. We have also found that the fingernail coloration saturates at lower force levels than the surrounding skin.

This paper presents an alternative approach: an external camera system that provides a fuller imaging of the back of the fingertip. The use of an external camera system presents challenges of keeping the fingernail in view, the lighting environment, and registration. None of these challenges is an issue with the photoplethysmograph sensor, since the sensor is fixed to the back of the nail and the lighting environment is controlled. Nevertheless, the high resolution of the fingernail image and surrounding skin is an offsetting advantage pro-

viding that these challenges can be met. Furthermore, the external camera approach does not encumber a subject and there is no need for sensor fabrication and individual fitting. The existence of low-cost cameras and of image processing methods readily performed on PCs makes the instrumentation costs of such an approach relatively low.

In this paper, we consider a fixed fingertip pressing against a 6-axis force sensor and imaged by a camera system in a controlled lighting environment. We do not yet consider issues of finger tracking or of handling variable lighting environments. The reason is to explore the fundamental effect of fingertip force versus fingernail coloration, without yet throwing in such complicating factors. We present results regarding the dependence of force range on the region of the fingernail and surrounding skin. A Bayesian estimation method is developed to predict fingerpad force from coloration changes. Preliminary results of force prediction accuracy for normal and shear forces separately are presented.
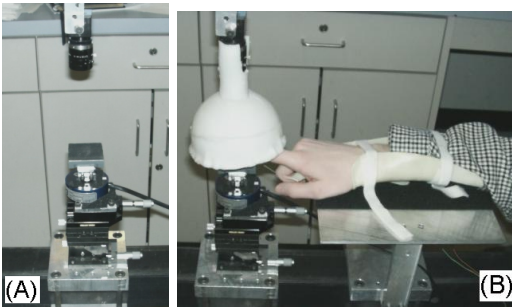
## 2 Calibration Stage



Figure 3: (A) A Flea 2D high-resolution camera images a contact plane mounted on a 6-axis JR3 force sensor and manual Cartesian stage. (B) Dome light and a molded plastic arm supporter with Velcro strips to provide arm fixation.

Figure 3 shows a calibration stage comprised of a 6-axis JR3 force sensor mounted on a small manual Cartesian stage, a Flea CCD video camera (Point Grey Research, Inc), and a small light dome. A rubber-surface flat plane is mounted on the JR3 force sensor to provide a contact surface; the Cartesian table is adjusted to locate the contact plane beneath a subject's fingertip. The subject's arm is fixated by a molded plastic arm support and Velco strips; the plastic arm has 2 DOFs for position adjustment. A subject sits in a chair adjustable with 4 DOF for positioning relative to the experimental stage.

The small light dome provides a controled lighting enviroment so that the images taken at different times are comparable. A reflective hemisphere was created from molded pastic; a hole at the top permits visual access by the Flea camera. LEDs placed along the perimeter reflect off the dome to create uniform lighting on the fingernail surface and to avoid specular reflection.

Images are captured from the Flea camera at 30 fps, synchronously with recorded forces from the JR3 force sensor. In combination with the lens, the Flea camera measures an image that is about 8 cm along the optical axis and is about 4x3 cm in crossection. The green channel from the camera's RGB color space has been found to produce a larger coloration response and better linearity with force than the other color channels, and is used subsequently.
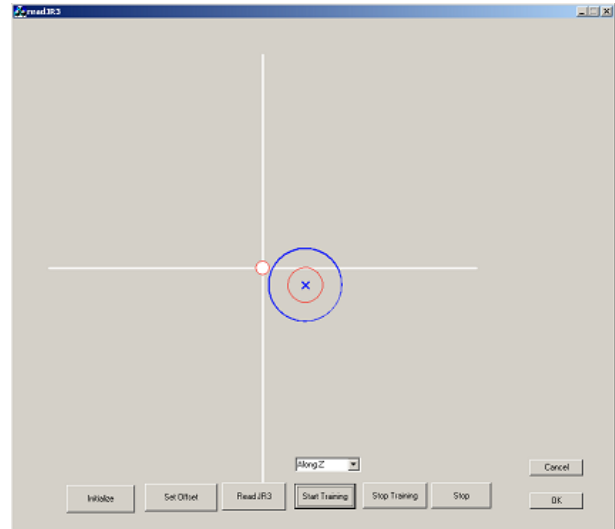


Figure 4: The display feedback.

A visual display (Fig. 4) guides subjects for calibration. Two of the three dimensions of force read from the JR3 force sensor are represented by position, while the third dimension is represented by the radius of a circle. Colors are used in the actual display. There is a blue circle with a blue cross in the center to represent the actual force applied, as measured by the JR3 force sensor beneath the finger. The $x$ position of the cross represents lateral shear force $F_x$, the $y$ position represents longitudinal shear force $F_y$, and the size of the circle represents the normal force $F_z$. The $x$ position of a white-filled red-edge sphere represents the desired shear force $F_x$ and the $y$ position represents desired shear force $F_y$. The circle size of the red circle, whose center follows the cross, represents the desired normal force $F_z$.

## 3 Image Registration and Surface Modeling

Fingernail locations will vary depending on the grasp and on the relative locations of the camera. As a particular fingernail is imaged, it will be necessary to correspond points in the image to a reference image so that calibration results can be applied. The reference image will need to be a 3D surface model fitted to the fingernail, because the fingernails and surrounding skin are curved surfaces and the shapes of individual fingernails vary. After comparing different surface representations including polygonal meshes, B-spline surfaces, and quadric surfaces, we chose a dense triangle mesh model since they are easiest to adapt to fingernail geometry.

3D points that form the vertices of triangular meshes are obtained with a Bumblebee BB-HICOL-60 (Point Grey Research, Inc.) stereo camera (Figure 5(B)). Since the fingernail is smooth and relatively featureless, it is difficult for the stereo camera system to find corresponding points in the two images. A common computer vision method for such situations is structured light onto the surface, which is easy for stereo vision to match. We employ a Steminc SMM96355SQR laser module to create a 4-by-4 grid pattern. A 3D data cloud obtained from the stereo camera is shown in Figure 6(B).

We do not employ the Bumblebee stereo camera for the coloration measurements because its resolution is too low.
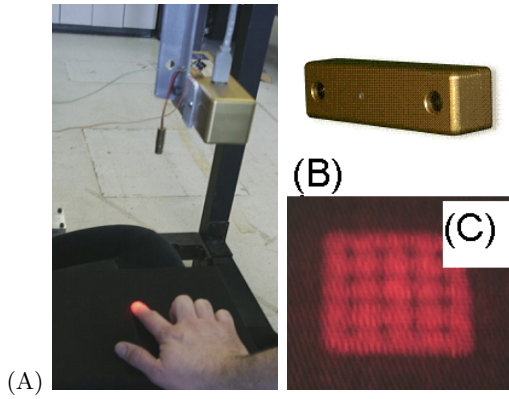
Figure 5: (A-B) The Bumblebee stereo camera. (C)The grid pattern that is projected onto the fingernail by the laser module.

However, its output is adequate for determining a 3D mesh model. To map the high-resolution Flea 2D images to a 3D model, we employ a well-known technique from computer vision [2] of adding fiducial marks to the fingernail and surrounding skin with a black marker (Figure 6(A)). It is necessary that the relative locations of the fiducial markings in the 3D model be known; this knowledge is obtained using the stereo camera. The fiducial marks are then automatically detected in the 2D image from the Flea camera [13] and used to compute the extrinsic parameter matrix $[\mathbf{R} \ \mathbf{t}]$, where $\mathbf{R}$ and $\mathbf{t}$ are the rotation and displacement from the 2D image to the coordinates of the 3D model (Figure 7).

The homogeneous coordinates of a point $i$ in the 2D image $\mathbf{p}_i$ and in the 3D model $\mathbf{P}_i$ are

$$\mathbf{p}_i = [u_i \ v_i \ 1]^T \qquad \mathbf{P}_i = [X \ Y \ Z \ 1]^T$$

where the 2D camera coordinates are $(u_i, v_i)$. Let $\mathbf{K}$ be the intrinsic parameter matrix for the camera, and define the 3x4 transformation

$$\mathbf{M} = \mathbf{K} [\mathbf{R} \ \mathbf{t}] = [\mathbf{m}_1 \ \mathbf{m}_2 \ \mathbf{m}_3]^T$$

The transform relation between the two coordinates is $\mathbf{p}_i = \mathbf{M} \, \mathbf{P}_i$. Hence

$$\mathbf{m}_1^T \mathbf{P}_i - (\mathbf{m}_3^T \mathbf{P}_i) u_i = 0 \qquad (1)$$
$$\mathbf{m}_2^T \mathbf{P}_i - (\mathbf{m}_3^T \mathbf{P}_i) v_i = 0 \qquad (2)$$

With 6 fiducial marks, the parameters in $\mathbf{M}$ can be calibrated with linear least squares. A registration result is shown in Figure 6(C).

## 4   Coloration Response

Figure 8 shows the coloration response $h_i$ of one typical point $i$ in the fingernail to a normal force $f_i$ on the finger pad. The response curve shows that the coloration starts to change when the force reaches a certain level $f_a$ and then stops changing at force $f_b$ because of saturation. Point $i$ can only transduce the force in the measurement range $[f_a, f_b]$.

To find the measurement range, the gradient curve of the response curve is calculated.

1. Locally weighted linear regression is used to fit the response curve [9]. The weighting function is $w_k =$
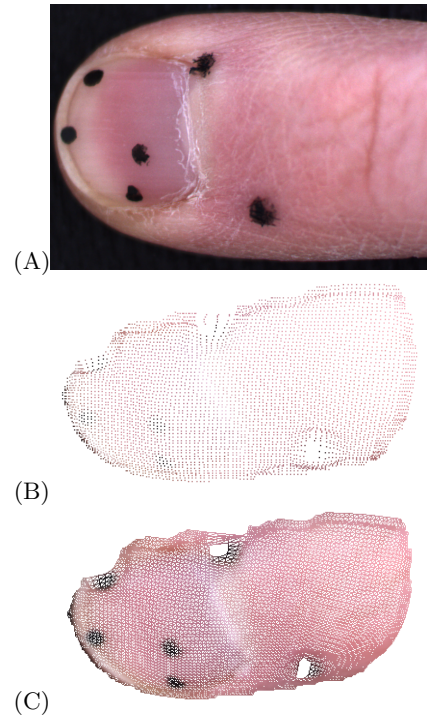


Figure 6: (A) Fingernail with fiducial marks. (B) 3D point cloud from the stereo camera. (C) Triangular 3D mesh with color mapped from the 2D image.

$exp(-D(f_k, f_i)^2/K_w^2)$, where $i$ is the index of the query point, and $k$ is the index of points around $i$. It gives larger weight to the points close to the query point and small weights to far points. This curve fitting emphasizes local information, which can pick up turning points. A typical result is shown in Figure 8.

2. Local gradients on the fitted curve are calculated by differentials.

3. A threshold $g_{th}$ is set. The crossing points where the gradient curve crosses the threshold are found. The measurement range $[f_a, f_b]$ is the segment that starts from a rising crossing point and stops at a falling crossing point, as shown in Figure 9.

Different points in the fingernail and surrounding skin have different measurement ranges. Some of them start from 0 N force, and some of them start from a relatively high force such as 4N. Some of them saturate at a very high force such as 10N, and some of them saturate at a lower force such as 3N. Some have two or more measurement ranges as show in Figure 10. Currently, the largest measurement range of the point is defined as the measurement range of that point.

Figure 11 shows the start point color map (left column) and the saturation point color map (right column) of one subject. The row numbers 1 to 7 represent the force levels [0, 1), [1, 2), [2, 3), [3, 4), [4, 5), [5, 6) and [6, 10) respectively. The dark points in each figure are the regions of the fingernail and surrounding skin with the associated force levels.

- Most points in the front of the fingernail start to respond at a force level of 2–3 N and saturate at 5–6 N.
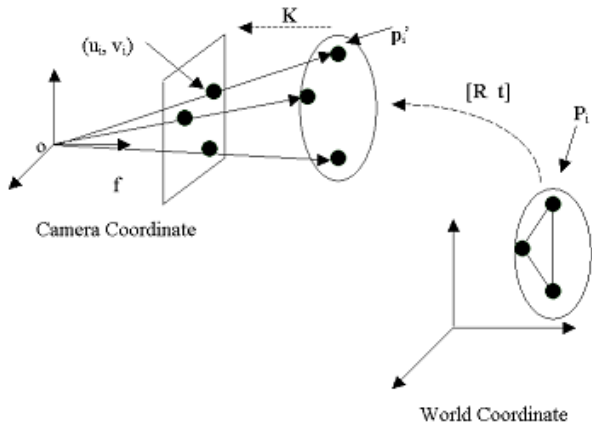
127

Figure 7: Perspective camera geometry model. A fiducial point is related between the 2D Flea camera image and the 3D surface model that defines the world coordinates.
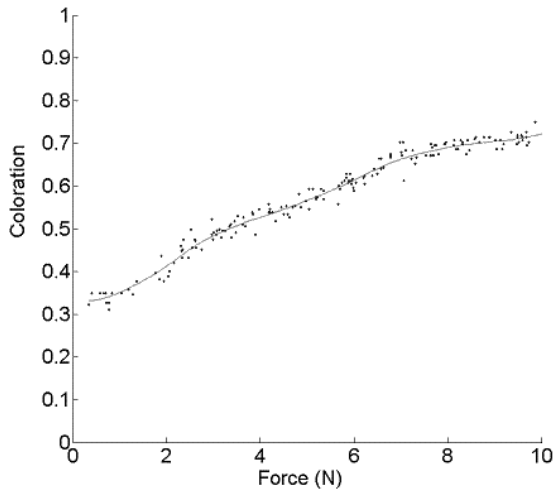


Figure 8: The coloration response data of a point in the fingernail with force from 0–10 N. A fitting curve is calculated with locally weighted linear regression.
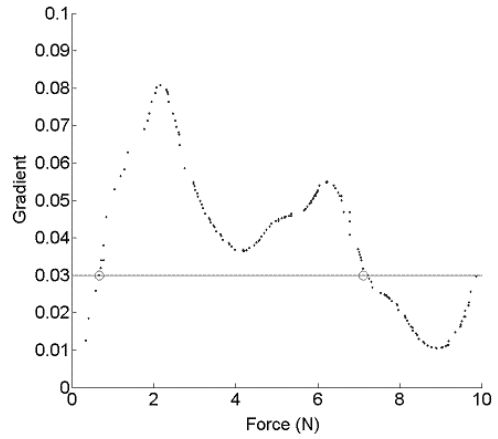


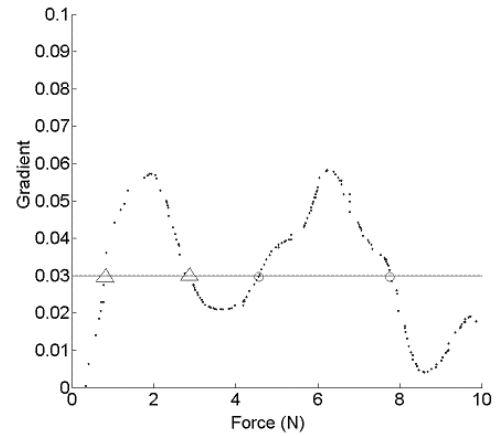Figure 9: The gradients and the crossing points (circles) when the threshold $g_{th} = 0.3$.



Figure 10: Two measurement ranges for this particular point on the fingernail.

- Most areas in the middle of fingernail start to respond at 0–1 N. Some of those areas saturate at 1–2 N, while others saturate at 2–3 N.

- Some areas on the skin surrounding the fingernail start to respond at 3–4 N and some start to respond at 4–5 N. They all saturate at force larger than 6 N.

There is no point on the fingernail or the surrounding skin which has a measurement range to cover 0–10 N. Some areas have their measurement range at low level forces, other areas have measurement ranges at high level forces. By combining all the area together, the fingernail coloration can possibly transduce forces from 0 to 10 N for this subject.

## 5   Linear Response Regions

Our research has identified that certain areas of the fingernail show a strong linear response of coloration to fingertip force, others do not. Not just the fingernail areas show this effect, certain areas of the surrounding skin show a strong linear response as well. The location of the good areas depends on the contact conditions. Figure 12 shows the areas that respond well to the sideways shear $f_x$, the forward shear
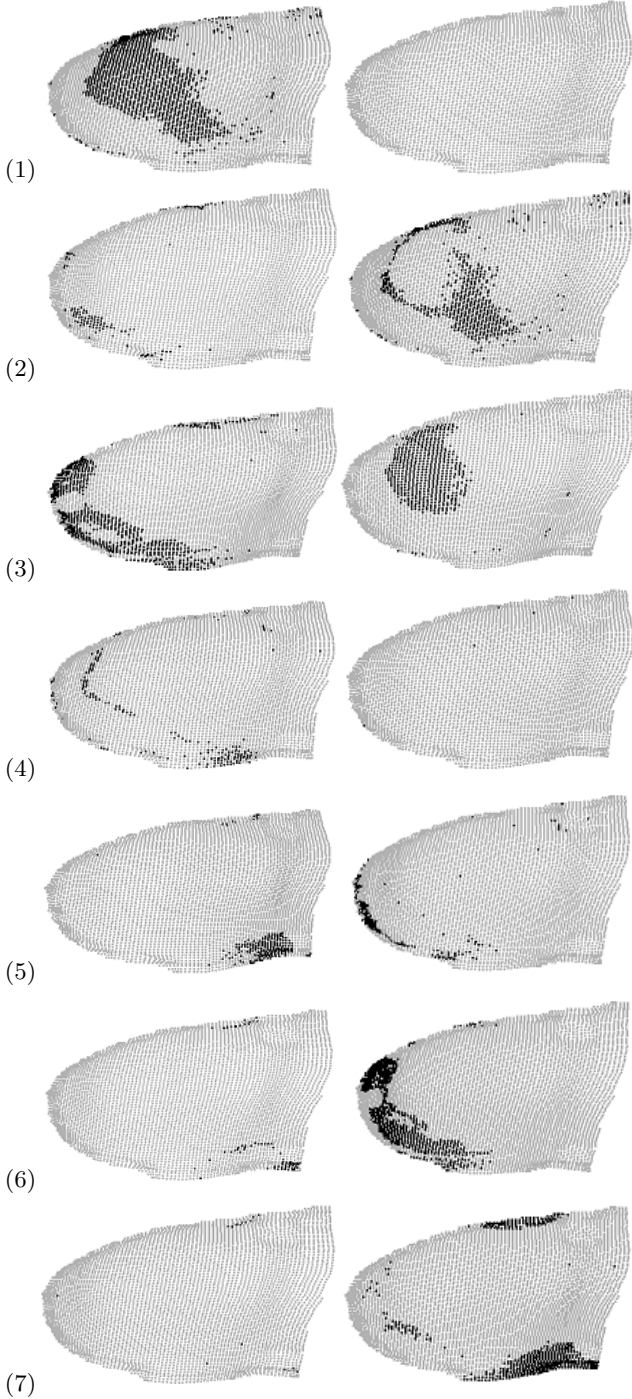
$f_y$, and the normal force $f_z$. Some areas respond well to all components of force, other areas are unique to a force component particularly for sideways shear $f_x$, where skin areas are particularly involved.
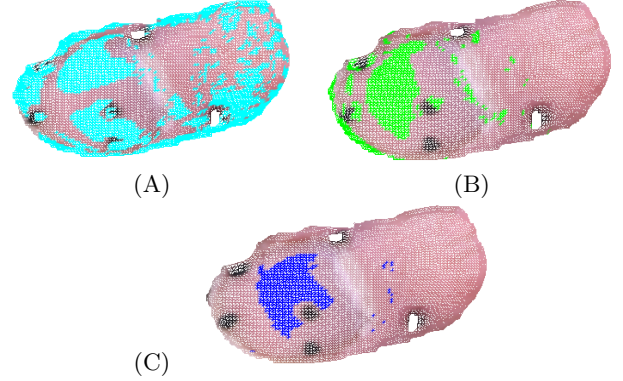


(A)　　　　　　　　(B)

(C)

Figure 12: Regions of the finger with good linear response to (A) sideways shear $f_x$, (B) forward shear $f_y$, and (C) normal force $f_z$.

The determination of which regions of the fingernail and surrounding skin respond well is done by a linear correlation analysis [1]. A linear model of intensity $h_i$ of a mesh element $i$ versus a force component $f_i$ was fit:

$$h_i = \alpha f_i + \beta; \tag{3}$$

where $a$ and $b$ are the linear fitting parameters. The correlation coefficient was computed for $n$ readings to determine how linear each mesh element response is with force.

$$R = \frac{\frac{1}{n}\sum_{i=1}^{n}(f_i - \bar{f})(h_i - \bar{h})}{\sqrt{\frac{1}{n}\sum_{i=1}^{n}(f_i - \bar{f})^2 \frac{1}{n}\sum_{i=1}^{n}(h_i - \bar{h})^2}} \tag{4}$$

$\bar{f}$ and $\bar{h}$ are the averages of the force and intensity readings respectively. Mesh elements whose correlation magnitudes are above 0.6 are considered to be good. Other mesh elements are discarded in order to reduce the dimensionality of the calibration model and to improve the calibration accuracy.

## 6　Bayesian Prediction Model

A good prediction model should be able to include all the statistical information. For this particular application, the model should include all the mesh elements with their measurement ranges. A least squares model cannot include the measurement ranges. Also, the number of input variables (the mesh elements) is too big for a traditional least squares model. A principle component analysis has to be done to reduce the number of variables, which throws out information. A least squares model would treat color as the input variable and force as the output variable. However, the causality is in the other direction: force causes color changes. A Bayesian model [11] captures this notion through the posterior $p(f|\mathbf{h})$, which can easily include the measurement range infomation.

Lump the $m$ coloration readings from the good regions into a vector $\mathbf{h} = [h_1 \ldots h_m]^T$. Bayes' rule is

$$p(f|\mathbf{h}) = \frac{p(\mathbf{h}|f)p(f)}{p(\mathbf{h})} \tag{5}$$



(1)

(2)

(3)

(4)

(5)

(6)

(7)

Figure 11: The start map (left column) and the saturation map (right column).

where $p(f)$ is the probability of a force component, $p(\mathbf{h})$ is the probability of the coloration observation, $p(\mathbf{h}|f)$ is the conditional probability of a coloration observation given a force, and $p(f|\mathbf{h})$ is the conditional probability of a force given a coloration observation. A key facilitator is that residuals of the coloration observations $\mathbf{h}$ given a force can be modeled using a normal distribution [11], which was verified using Q-Q plot [3].

$$p(\mathbf{h}|f) = \frac{1}{K} \exp{-\frac{1}{2}(\mathbf{h}-\overline{\mathbf{h}})^T \mathbf{\Sigma}^{-1}(\mathbf{h}-\overline{\mathbf{h}})} \qquad (6)$$

where $\overline{\mathbf{h}}$ is the mean of $\mathbf{h}$, and $\mathbf{\Sigma}$ is the variance matrix of $\mathbf{h}$, which can be estimated from the experimental samples of $\mathbf{h}$. $K$ is a constant which later cancels out. We assume the distribution of forces on the finger pad is uniform in the measurement range $[f_a, f_b]$:

$$p(f) = \begin{cases} \dfrac{1}{f_b - f_a} & f_a \leq f \leq f_b \\ 0 & \text{otherwise} \end{cases} \qquad (7)$$

The conditional probability of a force given a coloration observation can be written as

$$
\begin{aligned}
p(f|\mathbf{h}) &= \frac{p(\mathbf{h}|f)p(f)}{\int_{f_a}^{f_b} p(\mathbf{h}|f)p(f)df} \\[2mm]
&= \frac{\exp{-\frac{1}{2}(\mathbf{h}-\overline{\mathbf{h}})^T \mathbf{\Sigma}^{-1}(\mathbf{h}-\overline{\mathbf{h}})}}{(f_b - f_a)K \int_{f_a}^{f_b} p(\mathbf{h}|f)p(f)df} \qquad (8) \\[2mm]
&\equiv \frac{G(f,\mathbf{h})}{M(\mathbf{h})} \qquad (9)
\end{aligned}
$$

$M(\mathbf{h})$ is a constant, while $G(f,\mathbf{h})$ is a function of $f$ since the means $\overline{\mathbf{h}}$ depend on $f$. $\overline{h}_i$ is modeled as a linear function of $f$ as in (3), whose coefficients are estimated by linear regression.

A loss function is defined as

$$L(f,\hat{f}) = (f - \widehat{f})^2 \qquad (10)$$

The optimal Bayes estimation is

$$
\begin{aligned}
\hat{f}_{Bayes} &= \int_{f_a}^{f_b} f p(f|\mathbf{h})df \; / \; \int_{f_a}^{f_b} p(f|\mathbf{h})df \\[2mm]
&= \int_{f_a}^{f_b} f \, G(f,\mathbf{h})df \; / \; \int_{f_a}^{f_b} G(f,\mathbf{h})df \qquad (11)
\end{aligned}
$$

$\hat{f}_{Bayes}$ can be estimated by numerical integration with a coloration observation $\mathbf{h}$.

## 7  Calibration and Verification

To verify the system, experiments were carried out with 7 subjects varying in age, size, sex and race. Subjects used their index fingers to press on the rubber plate mounted on the JR3 force sensor while the camera monitored the coloration change of the index finger. Subjects were asked to produce normal forces and shear forces with display feedback. For each direction of force, 3 sets of data were taken. The first two sets were used for calibration and the third set was used for verification.

Figure 13 shows the verification examples of dynamic force applications for two subjects. Each subject is rhythmically exerting force on the calibration stage. For each subject, there are 3 plots representing 3 recordings of different tasks: exerting primarily a normal force $f_z$, a shear force $f_x$, or a shear force $f_y$. The Bayesian estimators are trained on a different set of recordings. The predictions are truncated above the 6 N force magnitude because of saturation of the coloration effect, even though the actual force production goes higher. For example, subject (A) produced a maximum of 25 N, which is why there is the big gap between cycles of the periodic force response. A total of 7 subjects were tested, and these plots are representative examples.
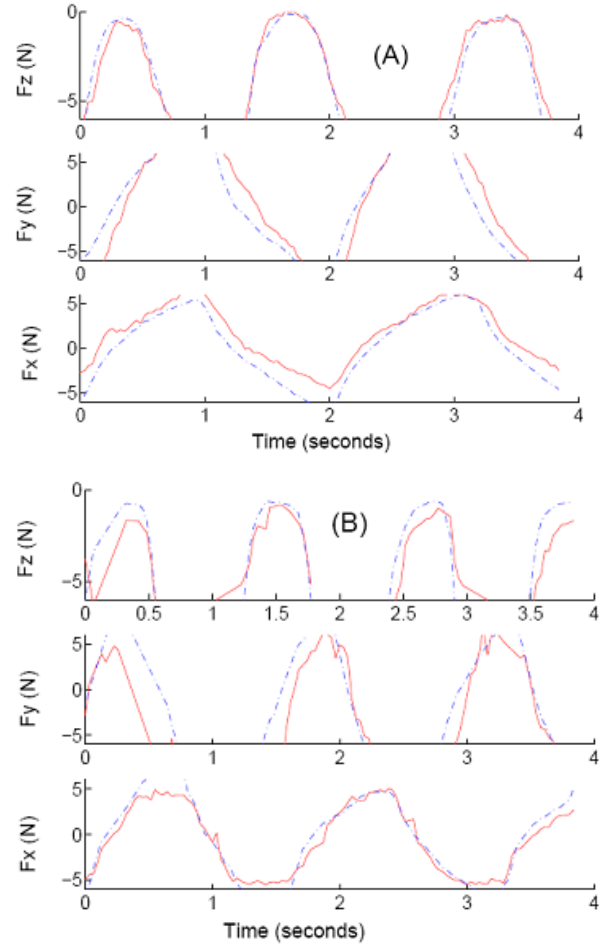


Figure 13: Force predictions for 2 subjects (A) and (B). For each subject there are 3 tasks: exerting primarily a normal force $f_z$, a shear force $f_x$, and a shear force $f_y$. The dashed lines represent the measured force components, the solid lines represent the estimated force component using the Bayesian predictor.

The accuracies of predicting the different force components vary between subjects and force directions. For the $z$ direction, 5 subjects have RMS error below 0.4, which is 6.7% of the measuring range, while the rest have RMS error below 0.8, which is 13% of the measuring range. For subject

(A) the normal force $f_z$ is predicted fairly accurately (RMS error is 0.34), whereas for subject (B) the sideways shear $f_x$ is predicted fairly accurately (RMS error is 0.278).

A statement of accuracy is complicated by delays in the coloration effect for this dynamic task. For example, the shapes of the actual versus predicted shear force profiles $f_y$ are fairly similar for subject (A), but they are displaced in time. If one looked at a particular instant in time, there might appear to be a large error between actual force and predicted force. Another complicating factor is that the Bayesian predictor was trained on the fast-ramp data, and time misalignment was not taken into account and no doubt has degraded the estimates. In comparison to the results of [8] using the photoplethysmograph fingernail sensor, our results are more accurate and double the range of forces that can be transduced, all the way up to the saturation level.

## 8 Discussion

The external camera system proposed in this paper shows a rather complex picture of coloration change with fingertip force. Depending on the region of the fingernail and surrounding skin, the usable force range varies. A typical example from a subject shows that the middle region of the fingernail has a low force range (0–2 N), the front region has an intermediate force range (2–6 N), and the surrounding skin has a high force range (3 to greater than 6 N). The saturation point varies with subject: sometimes less than 6 N, sometimes more. To predict the fingertip force response over the entire range from 0 N to saturation, readings from all fingernail and skin regions need to be combined.

The usable force range from our imaging system corresponds well to typical fingertip forces during contact. [10] reported that forces between 0 to 2 N are the most relevant for grasping and typing. [5] found that a human is capable of controlling a constant finger force in the range of 2 to 6 N with average error of 6% with visual feedback and natural haptic sense. Also, [6] found that the force that a human subject can comfortably apply for an extended time is about 3 N.

In view of these results, the limited sampling explains some of the limitations in force prediction of the photoplethysmograph sensor [6]. A few points on the nail were imaged, typically in the middle regions. This explains why the response appeared to saturate at 2 N. Also, the greater ability to select good response regions may partly explain the higher force prediction accuracies with the method of this paper. The Bayesian estimator may also yield greater accuracies than the least squares estimator in [6].

In this paper, the green color channel was used for coloration observation, since its response range and linearity is better than the blue and red channels. There are possibly other channels in other color spaces better than the green channel; one alternative, for example, is the HSI (hue saturation intensity) color space. Our future work will compare different coloration spaces.

The time course of the coloration affects the prediction accuracy. In the future, we will calibrate the time constant for each measurement point in the fingernail. The prediction model will only use the points with fast dynamic response in order to lessen the time course effect. The extent to which the different factors affecting coloration response (normal force, shear force, finger joint angle, etc.) can be separately estimated is also a subject of ongoing investigation.

## References

[1] J.S. Bendat and A.G. Piersol. *Engineering Applications of Correlation and Spectral Analysis.* Wiley, NY, 1980.

[2] A.G. Brown. A survey of image registration techniques. *ACM Computing Surveys,* 24:226-276, 1992.

[3] J.M. Chambers, W.S. Cleveland, B.Kleiner and P.A. Turkey. *Graphical Methods for Data Analysis.* Chapman & Hall/CRC Press, Boca Raton FL, 1983.

[4] D. Forsyth and J. Ponce. *Computer Vision - A Modern Approach.* Prentice Hall, 2003.

[5] L. A. Jones. Perception and control of finger forces. *Proc. ASME Dynamic Systems and Control Division,* 64:133-137, 1998.

[6] S.A. Mascaro and H.H. Asada. Photoplethysmograph fingernail sensors for measuring finger forces without haptic obstruction. *IEEE Trans. Robotics and Automation,* 17:698-708, 2001.

[7] S.A. Mascaro and H.H. Asada. Understanding of fingernail-bone interaction and fingertip hemodynamics for fingernail sensor design. *Proc 10th Intl. Symposium on Haptic Interfaces for Virtual Environment and Teleoperator Systems,* pp. 106-113, 2002.

[8] S.A. Mascaro and H.H. Asada. Measurement of finger posture and three-axis fingertip touch force using fingernail sensors. *IEEE Trans. Robotics and Automation,* 20:26-35, 2004.

[9] A.W. Moore, J. Schneider and K. Deng. Efficient locally weighted polynomial regression predictions. *Proc. International Machine Learning Conference,* Morgan Kaufmann Publishers, 1997.

[10] D.T.V. Pawluk and R.D. Howe. Dynamic lumped element response of the human fingerpad. *ASME J. Biomechanical Engineering,* 121(6):605-611, 1999.

[11] G.A.F. Seber and A.J. Lee. *Linear Regression Analysis.* Wiley, Hoboken NJ, 2003.

[12] J. K. Shim, M. L. Latash, V. M. Zatsiorsky, Prehension synergies in three dimentions. *J. Newrophysiol,* 93: 766-776, 2005.

[13] H.W. Trucco and V. Alessandro. *Introductory Techniques for 3-D Computer Vision.* Prentice Hall, 1998.